


Article

Near-Infrared Transitions from the Singlet Excited States to the Ground Triplet State of the S₂ Molecule

Lidan Xiao ^{1,*}, Bing Yan ¹ and Boris F. Minaev ^{2,3} 
¹ Institute of Atomic and Molecular Physics, Jilin University, Changchun 130012, China

² Department of Chemistry and Nanomaterials Science, Bohdan Khmelnytsky National University, 18031 Cherkasy, Ukraine

³ Department of Physics and Astronomy, Uppsala University, 752 36 Uppsala, Sweden

* Correspondence: xiaold19@mails.jlu.edu.cn; Tel.: +86-431-85168817; Fax: +86-431-85168816

Abstract: Intensity of transitions from the $b^1\Sigma_g^+$ and $a^1\Delta_g$ states to the ground state $X^3\Sigma_g^-$ in the near IR emission spectrum of the S₂ molecule has been calculated by the multireference configuration interaction method taking into account spin-orbit coupling (SOC). The intensity of the $b^1\Sigma_g^+ - X^3\Sigma_{g,Ms=\pm 1}^-$ transition is largely determined by the spin interaction with the electromagnetic wave, which comes from the zero-field splitting of the ground X multiplet and the SOC-induced mixing between b and $X^3\Sigma_{g,0}^-$ states. The Einstein coefficients for the experimentally detected 0–0, 0–1, 1–1 bands of the $b^1\Sigma_g^+ - X^3\Sigma_{g,Ms=\pm 1}^-$ emission system are calculated in good agreement with observations. The Einstein coefficient of the $a^1\Delta_g - X^3\Sigma_{g,Ms=\pm 1}^-$ magnetic dipole transition is very low, being equal to 0.0014 s^{-1} . Nonetheless, the weakest of all experimentally observed bands (the 0–0 band of the $a - X_{Ms=\pm 1}$ transition) qualitatively corresponds to this calculation. Most importantly, we provide many other IR bands for magnetic dipole $b^1\Sigma_g^+ - X^3\Sigma_{g,Ms=\pm 1}^-$ and $a^1\Delta_g - X^3\Sigma_{g,Ms=\pm 1}^-$ transitions, which could be experimentally observable in the S₂ transparency windows from a theoretical point of view. We hope that these results will contribute to the further experimental exploration of the magnetic infrared bands in the S₂ dimer.

Keywords: magnetic dipole transition; electro-quadrupole transition; S₂ molecule; near IR bands; Einstein coefficient



Citation: Xiao, L.; Yan, B.; Minaev, B.F. Near-Infrared Transitions from the Singlet Excited States to the Ground Triplet State of the S₂ Molecule. *Physchem* **2023**, *3*, 110–124. <https://doi.org/10.3390/physchem3010009>

Academic Editor: Andrzej Grzechnik

Received: 18 November 2022

Revised: 4 February 2023

Accepted: 7 February 2023

Published: 10 February 2023



Copyright: © 2023 by the authors. Licensee MDPI, Basel, Switzerland. This article is an open access article distributed under the terms and conditions of the Creative Commons Attribution (CC BY) license (<https://creativecommons.org/licenses/by/4.0/>).

1. Introduction

Diatomic sulfur as an important component of sulfur vapor has been widely studied by optical and microwave spectroscopy in laboratories at high temperatures near the sulfur melting point [1–4]. The dimer S₂ radical was also found in combustion processes, volcanic activity, and electric discharges through the sulfur vapor and sulfur-containing compounds [1–3,5]. At the same time, the S₂ molecule is one of the most important species in astrophysics. Compared with the research of O₂, the importance of the experimental spectral observation of S₂ cannot be ignored. For example, S₂ was monitored regularly, and it could track the star's apparent path in the sky through the images. It possesses a short lifetime due to ultraviolet (UV) photo-dissociation in space. Thus, the diatomic sulfur (S₂) radical has been detected in comet spectra [6,7]. Particularly, its emission is seen in the impact site of the comet Shoemaker-Levy 9 on Jupiter. For the same reason, the S₂ radical is an ideal monitor for behavior of a cometary nucleus. Moreover, the S gas was also found in the absorption spectrum of the Io's Pele plume against Jupiter by the Hubble Space Telescope in 1999 [8].

The quantum mechanical calculations of the spin-allowed electronic transitions in S₂ molecular spectra [9] and photo-dissociation dynamics [10–13] have been quite successful. In the well-known analogy of the dioxygen Schumann-Rung bands [14], the $B^3\Sigma_u^- - X^3\Sigma_g^-$ system of S₂ was studied by many authors [9–13].

Wieland et al. [15] have observed strong absorption bands of the S_2 molecule in the far UV region 160–187 nm, which were later reinvestigated [3] and classified as $C^3\Pi_u - X^3\Sigma_g^-$ and $D^3\Pi_u - X^3\Sigma_g^-$ transitions. In 1962, Tanaka [2] detected four systems of emission bands, all of which are of the $\Sigma-\Sigma$ type in the region 1760–2130 Å. They differ from the $C^3\Pi_u - X^3\Sigma_g^-$ and $D^3\Pi_u - X^3\Sigma_g^-$ strong bands [3] in the absorption of the S_2 molecule. It is known that the high vibrational energy levels of the $B^3\Sigma_u^-$ state are strongly predissociated by the crossing with the $B''^3\Pi_u$ state [4,9]. The presence of the $B^3\Sigma_u^- \leftarrow X^3\Sigma_g^-$ Schumann–Rung analogous bands system [10–13] and other optically allowed $B''^3\Pi_u - X^3\Sigma_g^-$ transitions [11] in the UV and visible regions of S_2 absorption spectra was investigated and interpreted [9]. In addition, there is one transient absorption in the far ultraviolet region that was assigned as the $f^1\Delta_u - a^1\Delta_g$ transition from a metastable state $a^1\Delta_g$ [13,16].

Four progressions of S_2 in the visible and near-infrared regions were observed using the laser-induced emission technique [17]; they were assigned as the $c^1\Sigma_u^- - X^3\Sigma_g^-$ and $c^1\Sigma_u^- - a^1\Delta_g$ transitions. According to the above, we know that many transition bands of S_2 have been observed; however, they are basically the transitions allowed by the electric dipole moment, and some weak transitions have not been mentioned. On the other hand, we find that the study of the transitions of S_2 molecules is still insufficient.

Both O_2 and S_2 are important components of astrophysics [6,7]. The spectral assignments that are based mainly on the vibrational spacings of the lower states and the electronic energy separations sometimes become difficult. Therefore, it is necessary to calculate some low-energy transitions. Thus, it is important to know as much as possible about their magnetic and electro-quadrupole properties. The intensity of the transitions was predicted by quantum mechanics, which would be complicated from a theoretical point of view since such evaluation of the method needs to take into account spin-orbit coupling, which leads to the admixture of wave functions for the different multiplet states.

The group VI A diatomic species O_2 and S_2 have the ground $X^3\Sigma_g^-$ state, the near-infrared $a^1\Delta_g$, and the red $b^1\Sigma_g^+$ counterpart of the $(\dots \sigma_g^2\pi_u^2)$ configuration [18–21]. Transitions between these states are strictly forbidden by electric dipole selection rules. However, they acquire weak magnetic dipole and electro-quadrupole transition moments due to spin-orbit coupling induced mixing of various electronic states [18,21]. Thus, the transitions between these states are easily obtained in the absorption and emission spectra of O_2 and S_2 molecules [17,22–25]. The $b^1\Sigma_g^+ - X^3\Sigma_g^-$ system is the analog of the atmospheric O_2 bands; it has been observed in emission in the near infrared using a discharge flow system in which metastable O_2 ($^1\Delta_g$) molecules sensitized the emission of the S_2 molecules [22]. The study of transitions is helpful to compare the electronic structures of the two molecules.

This procedure involves the spin-orbit matrix elements between $b^1\Sigma_g^+$ singlet and $X^3\Sigma_g^-$ triplet states of the S_2 molecule, which were obtained in a series of AO basis sets [20,21]. Transitions require accurate energy levels and transition moments to better reduce errors. The $b^1\Sigma_g^+$ state of S_2 could be efficiently quenched by collisions; it still produces the emission spectra of magnetic dipole $b^1\Sigma_g^+ - X^3\Sigma_{g,Ms=\pm 1}^-$ ($0-0, 0-1, 1-1$) transitions of S_2 which were measured by the Fourier-transform spectrometer at high resolution [22]. In addition, dating back to 1979, the weak emission spectra for the ($v' = 0$, $v'' = 0$) band of the magnetic dipole $a^1\Delta_g - X^3\Sigma_{g,Ms=\pm 1}^-$ transition was detected in the near-infrared region [23,24]. The intensity of the $a^1\Delta_g - X^3\Sigma_{g,Ms=\pm 1}^-$ band for a chemically unstable S_2 molecule is very low; its short radiative lifetime was calculated to be about 350 s (the Einstein coefficient $A = 0.00286 \text{ s}^{-1}$) [21]. At present, few studies have given a complete and accurate calculation of the electronic-state energy level and transition moment of the S_2 molecule. The current work makes up for the lack of predecessors and provides theoretical support for future generations.

The primary purpose of the present work is to study the intensity of parity-forbidden singlet-triplet (S-T) transitions between $X^3\Sigma_g^-$ and $a^1\Delta_g$, $b^1\Sigma_g^+$ states in the S_2 dimer using

the MRCI+Q method, which could explain how to overcome the spin-forbidden transition of the electric-dipole approximation taking into account spin-orbit coupling. Previous studies of the S₂ dimer have mainly focused on the UV and visible regions. In addition, the near-infrared $b^1 \Sigma_g^+ - X^3 \Sigma_{g,Ms=\pm 1}^-$ (0–0, 0–1, 1–1) and $a^1 \Delta_g - X^3 \Sigma_{g,Ms=\pm 1}^-$ (0–0) bands [22,25] have also been observed experimentally. The current work calculates the magnetic dipole moment of the $b^1 \Sigma_g^+ - X^3 \Sigma_{g,Ms=\pm 1}^-$ and $a^1 \Delta_g - X^3 \Sigma_{g,Ms=\pm 1}^-$ transitions of S₂ for other vibronic bands in the microwave–infrared regions, which could be observed from a theoretical point of view. The transition properties of the $b^1 \Sigma_g^+$ and $a^1 \Delta_g$ states with respect to the ground state $X^3 \Sigma_g^-$ have been evaluated by SOC perturbations from the $^3\Pi_g$ and $^1\Pi_g$ states of the S₂ systems. We also note that the magnetic dipole $b^1 \Sigma_g^+ - X^3 \Sigma_{g,Ms=1}^-$ transition moment is decided by the spin part due to the zero-field splitting of the $X^3 \Sigma_g^-$ state [18–21]. The calculated magnetic dipole $a^1 \Delta_g - X^3 \Sigma_{g,Ms=1}^-$ transition only contains the orbital angular-momentum contribution [18]. In addition, the error source for the Einstein coefficient is discussed. It is most important that we successfully reproduce the experimentally observed magnetic dipole $b^1 \Sigma_g^+ - X^3 \Sigma_{g,Ms=\pm 1}^-$ and $a^1 \Delta_g - X^3 \Sigma_{g,Ms=\pm 1}^-$ vibronic bands in our efforts to obtain full predictions. The weak intensities of electro-quadrupole $a^1 \Delta_g - b^1 \Sigma_g^+$ and $a^1 \Delta_g - X^3 \Sigma_{g,Ms=0}^-$ bands are also investigated since they should exhibit a particular rovibronic structure. However, the results show that there is little hope that these quadrupole bands can be measured experimentally. Nevertheless, the present results may help further search for the magneto-infrared band in the S₂ systems.

2. Method of Calculations

The electronic structure calculation of S₂ has been carried out with the Molpro 2012 suite of the quantum chemical package [26]. The “aug–cc–pwCVTZ” basis set with diffuse s-type (0.018684493) and p-type (0.011220492) Gaussian functions is used for the S atom. There are two electrons (excluding the 1s² electron of S) participating in the MRCI calculation of S₂, and the corresponding active space is determined by eight molecular orbitals (MOs), including two σ_g , one π_u , one π_u , two σ_u , one π_g , and one π_g symmetry (3s²3p⁴). The SOC is considered with the aid of the state-interacting approach utilizing the Breit–Pauli operator. After taking the eigenfunction of the unperturbed \hat{H}_{el} Hamiltonian as the basis of diagonalization, the diagonalized $\hat{H}_{el} + \hat{H}_{so}$ matrix can obtain the eigenfunction and eigenvalue of the electronic state (Ω presentation).

The magnetic dipole operator M consists of two terms, which are spin (S) and orbital angular momentum (L); it is determined by

$$M = \frac{\mu_B}{\hbar}(L + g_e S) \quad (1)$$

where the electronic g -factor g_e is equal to 2.0023. Then, after taking the SOC into account, the singlet and the triplet states are mixed, and the perturbed wave function Φ of the electronic state is expressed as

$$\Phi_{x,Ms=0} = |X^3 \Sigma_{g,Ms=0}^- \rangle - C_{b,x}^* |b^1 \Sigma_g^+ \rangle \quad (2)$$

$$\Phi_{x,Ms=1} = |X^3 \Sigma_{g,Ms=1}^- \rangle + \sum_n C_{x,n} |n^1 \Pi_g \rangle \quad (3)$$

$$\Phi_b = |b^1 \Sigma_g^+ \rangle + C_{b,x} |X^3 \Sigma_{g,Ms=0}^- \rangle + \sum_n C_{b,n} |n^3 \Pi_{g,Ms=\pm 1} \rangle \quad (4)$$

$$\Phi_a = |a^1 \Delta_g \rangle + \sum_n C_{a,n} |n^3 \Sigma_{g,Ms=\pm 1} \rangle \quad (5)$$

where

$$C_{b,x} = \frac{\langle X^3 \Sigma_{g,Ms=0}^- | H_{SO} | b^1 \Sigma_g^+ \rangle}{E_b - E_x} \quad (6)$$

The mixing coefficient of the infrared band ($b^1 \Sigma_g^+ - X^3 \Sigma_{g,M_s=\pm 1}^-$ transition) is calculated as $C_{b,X} = 0.05504i$, which is derived from the SOC matrix element (426.53 cm^{-1}) and energy difference $\Delta E_{b-X} = 7749 \text{ cm}^{-1}$; the former is determined by the multiplet splitting for the $S(^3P)$ state.

The spin contribution of magnetic operator Equation (1), taking into account Equation (4), becomes

$$\begin{aligned} \langle \Phi_b | S_x | \Phi_{x,M_s=1} \rangle &= \frac{\langle b^1 \Sigma_g^+ | L_Z S_Z | X^3 \Sigma_{g,M_s=0}^- \rangle \langle X^3 \Sigma_{g,M_s=0}^- | S_x | X^3 \Sigma_{g,M_s=1}^- \rangle}{E_b - E_x} \\ &= i \frac{\langle b^1 \Sigma_g^+ | L_Z S_Z | X^3 \Sigma_{g,M_s=0}^- \rangle}{E_b - E_x} \end{aligned} \quad (7)$$

Besides the spin contribution, the contribution of the orbital angular momentum L to the magnetic dipole transition moment is also essential. Taking the orbital section of the $b^1 \Sigma_g^+ - X^3 \Sigma_{g,M_s=1}^-$ transition as an example, we obtain

$$\begin{aligned} \langle \Phi_b | L_- | \Phi_{x,M_s=1} \rangle &= \sum_n C_{X,n} \langle b^1 \Sigma_g^+ | L_- | n^1 \Pi_g \rangle + \sum_n C_{b,n}^* \langle n^3 \Pi_g | L_+ | X^3 \Sigma_{g,M_s=1}^- \rangle \\ &= \sum_n \frac{\langle n^1 \Pi_g | H_{so} | X^3 \Sigma_{g,M_s=1}^- \rangle \langle b^1 \Sigma_g^+ | L_- | n^1 \Pi_g \rangle}{E_x - E_n(n^1 \Pi_g)} \\ &\quad + \sum_n \frac{\langle n^3 \Pi_{g,M_s=1} | L_+ | X^3 \Sigma_{g,M_s=1}^- \rangle \langle b^1 \Sigma_g^+ | H_{so} | n^3 \Pi_{g,M_s=1} \rangle}{E_x - E_n(n^3 \Pi_g)} \end{aligned} \quad (8)$$

The role of the intermediate $^3\Pi_g$ and $^1\Pi_g$ states is to establish a connection between the singlet ($a^1\Delta_g$ and $b^1 \Sigma_g^+$) state and the triplet ground ($X^3 \Sigma_g^-$) state, allowing the S_2 molecule to arise from these magnetic transitions in the near-IR region. In addition, the intensity of the quadrupole transition moment is determined by

$$\langle a^1 \Delta_g | Q | \Phi_{x,M_s=0} \rangle = \langle a^1 \Delta_g | Q | X^3 \Sigma_{g,M_s=0}^- \rangle - C_{b,x}^* \langle b^1 \Sigma_g^+ \rangle = -C_{b,x}^* \langle a^1 \Delta_g | Q | b^1 \Sigma_g^+ \rangle \quad (9)$$

Here, Q is the quadrupole part of the multipole expansion of radiation. For different transitions, the formulas of the Einstein coefficient A have different expressions, Equations (10) and (11), corresponding to the magnetic dipole moment and the electro-quadrupole moment, respectively.

$$A = 0.2706 \times E^3 \times 10^{-10} \times M^2 \quad (10)$$

$$A = 1.1199 \times 10^{-22} \times Q^2 \times E^5 \quad (11)$$

The unit of energy E is cm^{-1} ; the magnetic dipole moment M , electric quadrupole moment Q , and Einstein coefficient A are in units of the Bohr magneton, ea_0^2 , and s^{-1} , respectively.

3. Results for the S_2 Molecule

3.1. Energy Calculations in the S_2 Spectrum

The potential energy curves (PECs) of the ground state ($X^3 \Sigma_g^-$), the low-lying excited states ($a^1\Delta_g$ and $b^1 \Sigma_g^+$), and the upper states ($d^1 \Sigma_g^+$, $1^3\Pi_g$, and $1^1\Pi_g$) of S_2 have been calculated using the MRCI+Q method and are plotted in Figure 1. On the ground of these PECs, the spectroscopic constants of the bound Λ -S states—including adiabatic excitation energy T_e , equilibrium internuclear distance R_e , vibrational frequency ω_e , anharmonic constant $\omega_e x_e$, and rotational constant B_e —are also listed in Table 1. At present, many scholars have studied these constants [9,20,27–38], and we only list representative data for comparison.

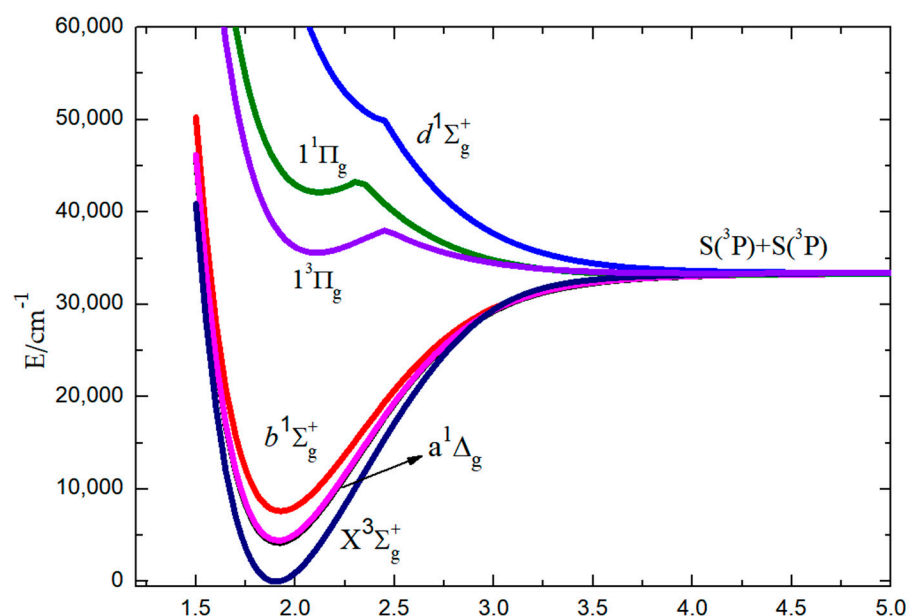


Figure 1. Potential energy curves of the low-lying “gerade” Λ -S states for S_2 calculated at the MRCI level.

Table 1. Spectroscopic constants for the Λ -S states of S_2 .

	T_e/cm^{-1}	$R_e/\text{\AA}$	ω_e/cm^{-1}	$\omega_e\chi_e/\text{cm}^{-1}$	B_e/cm^{-1}
$X^3\Sigma_g^-$	0	1.9027	709.6586	2.8198	0.2913
		1.889 Expt [37]	725.65 Expt [37]		
		1.90 [38]	760 [38]		
		1.8960 [9]	729 [9]	3.2096 [9]	0.2933 [9]
$a^1\Delta_g$	4459.3688	1.9150	682.6867	3.0585	0.2876
		1.898 Expt [37]	702.35 Expt [37]		
		1.907 [38]	746 [38]		
		1.9058 [9]	703 [9]	3.2536 [9]	0.2903 [9]
$b^1\Sigma_g^+$	7649.5722	1.9249	650.8639	2.8708	0.2843
			669.7 Expt [37]		
		1.914 [38]	732 [38]		
		1.9181 [9]	674 [9]	3.3856 [9]	0.2866 [9]
$1^3\Pi_g$	35,619.7022	2.1081	435.4006	7.7393	0.2373
$1^1\Pi_g$	42,170.9966	2.1213	459.4193	6.7306	0.2342

It can be seen that the calculated R_e values of the $X^3\Sigma_g^-$ ground state and low-lying $a^1\Delta_g$ excited state are in relatively good agreement with the corresponding previous experimental [37] and theoretical [9,38] data. Compared with the experimental ω_e values for the $X^3\Sigma_g^-$, $a^1\Delta_g$, and $b^1\Sigma_g^+$ PECs, our results are a bit lower, and the differences are 15.99 cm^{-1} (2.25%), 19.66 cm^{-1} (2.88%), and 18.84 cm^{-1} (2.89%), respectively [37].

In addition, the complete basis set (CBS) limit for vertical excitation energy was calculated with the following extrapolation schemes, which use two- or three-point extrapolation formulas. Three-point extrapolation generally underestimates the limit,

$$E_n = E_{\text{CBS}} + Be^{-(n-1)} + Ce^{-(n-1)^2} \quad n = (3, 4, 5)$$

Two-point extrapolation typically overestimates it,

$$E_n = E_{\text{CBS}} + \frac{B}{n^3} \quad n = (4, 5)$$

The reliability of vertical excitation energy in quantum chemistry is evidently dependent on the basis set. The optimized results are obtained from complete basis set calculations. We expect them to be more accurate than other results [21,38]. In Table S1, the influence of the AO basis is negligible for the vertical excitation energy, as can be seen from the results obtained by employing two- or three-point extrapolation formulas in different bases. The maximum difference of the vertical excitation energy from $X^3\Sigma_g^-$ state to the $a^1\Delta_g$, $b^1\Sigma_g^+$, $1^3\Pi_g$, $1^1\Pi_g$ states is only a few percent (1.10%, 2.96%, 0.51%, 0.16%).

The relative positions of the a and b levels are of crucial importance in our study. Experimental energy data for the gas phase T_0 and T_e values are 4394.2 and 4745.4 cm^{-1} for the $a^1\Delta_g$ state [23]. The T_0 value is close to other experimental data for Ne matrix (4395 cm^{-1}), where the light noble gas environment provides negligible perturbation for S_2 molecule [5]. Our T_0 value is a bit lower (4118 cm^{-1}) but the ratio of the T_0 energies of the $a^1\Delta_g$ and $b^1\Sigma_g^+$ states (0.562) is quite close to experimental data (0.551) [23] being also in accordance with the corresponding ratios 0.60, 0.56, and 0.54 observed for O₂, SO, and Se₂, respectively [39].

3.2. Magnetic Dipole Mechanisms for the $X^3\Sigma_g^- - a^1\Sigma_g, b^1\Sigma_g^+$ Transitions in the S_2 Spectrum

Transitions between the low-lying “gerade” states are forbidden by dipole selection rules ($\Delta\Lambda = 0, \pm 1$, $\Delta S = 0$, $g \rightarrow u$), but SOC-induced mixing between electronic multiplets provides additional source of weak magnetic dipole transitions (which satisfy the selection $\Delta\Lambda = 0, \mp 1$, $\Delta S = 0$, $g \rightarrow g$, $u \rightarrow u$) in the near-infrared region of the S_2 spectrum.

The calculated {1}–{6} transitions between $a^1\Delta_g$, $b^1\Sigma_g^+$, and $X^3\Sigma_g^-$ states are collected in Figure 2; these transitions can be detected as weak magnetic and quadrupole bands. What we want to stress is that the weak intensity of the vibrational near-IR band in the S_2 spectra can be measured at the liquid-nitrogen-cooled germanium detector facilities [22]. Among them, the {3} transition can be expressed as the difference in the quadrupole moments between a and X states multiplied by the corresponding $C_{a,x}$ coefficient. However, the actual calculation leads to neglected electro-quadrupole transition {3} intensity. The magnetic S-T transition moment number {2} “borrows” intensity from transition number {4} ($X^3\Sigma_{g,Ms=0}^- - X^3\Sigma_{g,Ms=1}^-$); this is a typical EPR {4} transition moment equal to two Bohr magnetons ($2\mu_B$) in zero magnetic fields, which can be considered as the contribution of the spin magnetic dipole from nature. In addition, the orbital angular-momentum operator also contributes to the S-T transition {2} intensity. A similar orbital analysis is also applied to the transition number {1} intensity, which is dominated by the orbital magnetic interaction. According to perturbation theory, the SOC mixing of the electronic states is responsible for “intensity borrowing” of transition numbers {1} and {2}. Transition {5} is dominated by the contribution of the orbital magnetic dipole, and the intensity of magnetic dipole moment transition {5} is very weak, almost negligible.

In Table S2, three different sets, basis A (aug-cc-pwCVTZ), basis B (aug-cc-pwCVQZ), and basis C (aug-cc-pwCV5Z), have been employed in order to obtain more accurate spin-orbit matrix elements, which are responsible for the discussed intensity borrowing schemes. The difference between basis X ($X = A, B, C$) and basis X_1 ($X_1 = A_1, B_1, C_1$) is that X_1 correlates the $2s^22p^63s^23p^4$ electrons of the S atom to account for the core-valence (CV) effect. Its result shows that the impact of the CV effect cannot be ignored in the calculation process. Basis A_2 contains additional diffuse s-type (0.018684493) and p-type (0.011220492) Gaussian functions relative to basis A_1 in order to better understand the influence of the CV effect and diffusion function on spin-orbit coupling matrix elements, which indicates that the effect of the diffusion function is tiny or even negligible.

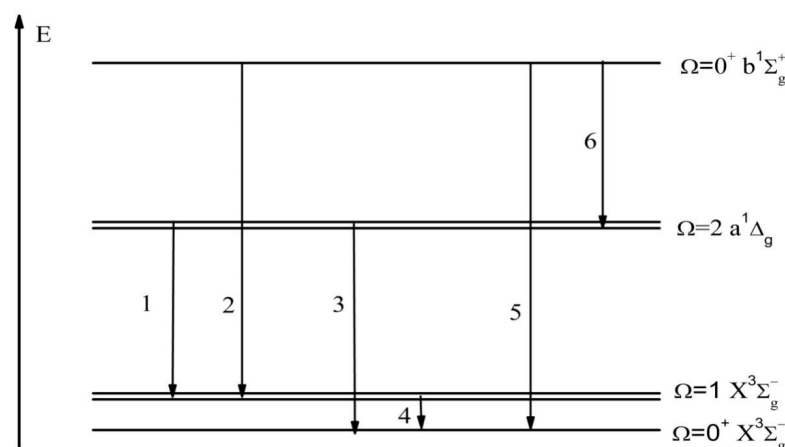


Figure 2. Numbering of forbidden electronic transitions in the NIR region of S_2 emission. (Transitions 1, 2, 4, and 5 represent magnetic dipole transition moments. Transitions 3 and 6 represent electric quadrupole transition moments).

In Table 2, it is obvious that the best CBS limit produces spin-orbit matrix elements with the $X^3\Sigma_g^-$ and $b^1\Sigma_g^+$, $1^1\Pi_g$, $1^3\Pi_g$ states which are slightly higher than the previous theoretically calculated values [20,40]. However, our values are within a reasonable error range. The best CBS limit results for spin-orbit matrix elements between the $1^3\Pi_g$ and $a^1\Delta_g$, $b^1\Sigma_g^+$ states are predicted to be close to the result of basis G; the differences are 5.90% and 6.39%, respectively.

Table 2. Calculated spin-orbit matrix elements in S_2 ($R_{s-s} = 1.899 \text{ \AA}$).

Basis	Spin-Orbit Matrix Elements with the $X^3\Sigma_g^-$ State for Other States (cm^{-1})			Spin-Orbit Matrix Elements with the $1^3\Pi_g$ State for Other States (cm^{-1})	
	$b^1\Sigma_g^+$	$1^1\Pi_g$	$1^3\Pi_g$	$a^1\Delta_g$	$b^1\Sigma_g^+$
best CBS	429.85 ± 0.17	215.90 ± 0.06	-217.38 ± 0.01	-212.76 ± 0.02	201.47 ± 0.00
basis D [20,41]	422.5	200.3	−203.1		
basis D1 (core2) [20]	423.0	202.7	−204.0		
basis E [20]	410.3	200.9	−200.8		
basis F [20]	416.6	203.9	−204.9		
basis G (core2) [21]				−200.2	188.6

Basis D is the double-zeta set for sulfur given; basis D1: on the basis of basis D, correlating the $2s^2 2p^6 3s^2 3p^4$ electrons of S atoms to account for the CV effect of the S_2 . Basis E contains additional s and p bond functions {exponents $\alpha(s) = 1.0$ and $\alpha(p) = 0.6$ } relative to basis D; basis F adds only an s bond function to basis D. Basis G consists of the double-zeta (12s, 9p) set for sulfur contracted to (s, 4p) with s and p bond functions {exponents $\alpha(s) = 1.0$ and $\alpha(p) = 0.6$ }.

The calculated spin-orbit matrix elements between the Ω - Ω states of the S_2 system (Figure 3) show very interesting R dependence behavior. For example, the SOC integral $\langle b^1\Sigma_g^+ | L_y S_y | 1^3\Pi_{g,M_s=1}^x \rangle$ is a rising function with R while the important matrix element $\langle b^1\Sigma_g^+ | L_z S_z | X^3\Sigma_{g,M_s=0}^- \rangle$ declines with $R > R_0$. The SOC integrals $\langle b^1\Sigma_g^+ | L_y S_y | 1^3\Pi_{g,M_s=1}^x \rangle$ and $\langle b^1\Sigma_g^+ | L_x S_x | 1^3\Pi_{g,M_s=1}^y \rangle$ are equal. The spin-orbit interaction operator subscript ($L_y S_y$) and state superscript ($1^3\Pi_{g,M_s=1}^x$) are defined as y components of the SOC operator and x components of the degenerate irreducible representation Π_g , respectively. At the same time, it is clearly visible that the value of the SOC integral $\langle b^1\Sigma_g^+ | L_z S_z | X^3\Sigma_{g,M_s=0}^- \rangle$ is the largest, which is one of the reasons why the magnetic dipole moment $b^1\Sigma_g^+ - X^3\Sigma_{g,M_s=1}^-$ transition intensity is much stronger than other transitions.

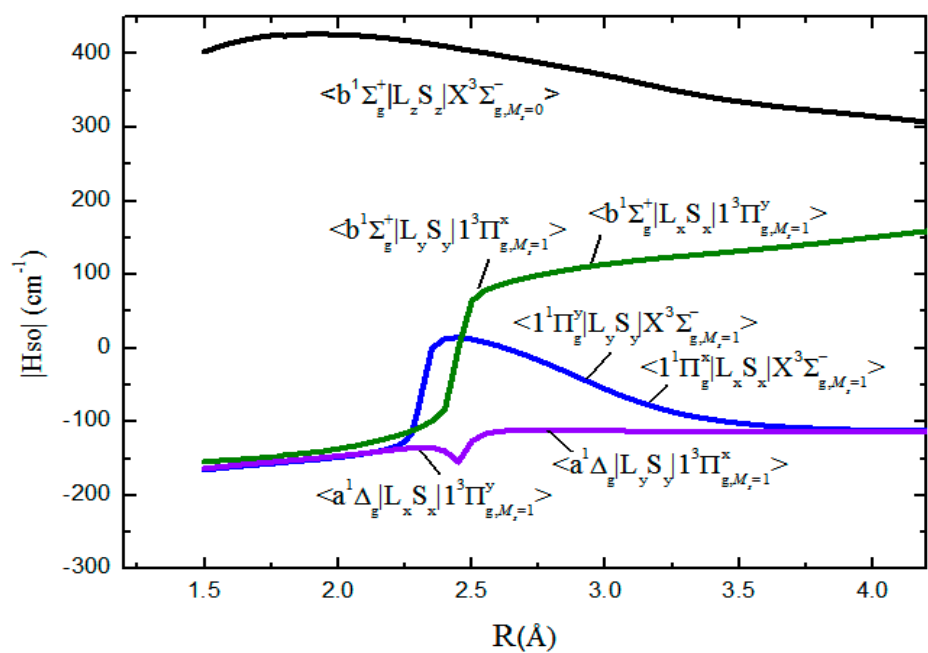


Figure 3. R dependence of spin-orbit matrix elements of the Ω-Ω states for S₂.

The calculated orbital angular-momentum parts are necessary for the magnetic dipole transition intensity estimations, which are collected in Table 3, while the corresponding theoretically calculated values of the reference are also listed. They show that the difference in orbital transitions between states range from 0.26% to 3.72% at the equilibrium internuclear distance ($R_{s-s} = 1.899 \text{ \AA}$). Among them, the $\langle a^1\Delta_g | L_x | 1^1\Pi_g^y \rangle$ transition has the largest difference between our results and the calculated values of Ref. [21], which is about 3.72%.

Table 3. Calculated values of the L matrix elements (in atomic unit (a.u.)) for the quantities that are necessary for calculation of the magnetic transition probabilities in S₂.

$R_{s-s} \text{ (\AA)}$	$\langle b^1\Sigma_g^+ L_x 1^1\Pi_g^y \rangle$	$\langle b^1\Sigma_g^+ L_y 1^1\Pi_g^x \rangle$	$\langle 1^3\Pi_{g,Ms=1}^x L_x X^3\Sigma_{g,Ms=1}^- \rangle$
1.8	1.23995	1.23995	1.19769
1.85	1.25557	1.25557	1.20622
1.899	1.25986/1.26317 [21]	1.25986/1.26317 [21]	1.21257/1.22810 [21]
1.95	1.25704	1.25704	1.21662
2.0	1.25890	1.25890	1.21828
2.05	1.25894	1.25894	1.21742
2.1	1.25751	1.25751	1.21392
$R_{s-s} \text{ (\AA)}$	$\langle a^1\Delta_g L_x 1^1\Pi_g^y \rangle$	$\langle a^1\Delta_g L_y 1^1\Pi_g^x \rangle$	$\langle 1^3\Pi_{g,Ms=1}^y L_y X^3\Sigma_{g,Ms=1}^- \rangle$
1.8	1.21115	1.21115	1.19769
1.85	1.21464	1.21464	1.20622
1.899	1.21624/1.26317 [21]	1.21624/1.26317 [21]	1.21257/1.22810 [21]
1.95	1.21697	1.21697	1.21662
2.0	1.21202	1.21202	1.21828
2.05	1.20255	1.20255	1.21742
2.1	1.18724	1.18724	1.21392

In Table 4, the spin and orbit contributions to the total magnetic dipole transition moments between the $X^3\Sigma_g^-$ and $a^1\Delta_g$, $b^1\Sigma_g^+$ states in the S₂ spectrum are given; see also Figure 4 for details. The spin operator contribution to the magnetic $b^1\Sigma_g^+ - X^3\Sigma_{g,Ms=\pm 1}^-$ transition comes from the microwave band ($X^3\Sigma_{g,Ms=0}^- - X^3\Sigma_{g,Ms=1}^-$) and the $C_{b,X}$ coefficient. The intensity of the magnetic transition between spin sublevels ($Ms = \pm 1 - Ms = 0$) of the ground triplet state $X^3\Sigma_g^-$ is equal to $2\mu_B$. The orbital part of the magnetic

$b^1\Sigma_g^+ - X^3\Sigma_{g,M_s=\pm 1}^-$ transition remains of the order of magnitude less than the spin-current part for R distances from 1.5 Å to 2.2 Å; in fact, it accounts for about one-seventh of the total $b^1\Sigma_g^+ - X^3\Sigma_{g,M_s=\pm 1}^-$ transition moment value. Note that the spin contribution in Table 4 must be multiplied by the g-factor value of the free electron $g_e = 2.0023$. In addition, the magnetic dipole $a^1\Delta_g - X^3\Sigma_{g,M_s=\pm 1}^-$ transition is mainly determined by the contribution of the orbital angular momentum L; it is equal to 0.026369 μ_B at R_e distance.

Table 4. Spin (S), orbit (L), and the total magnetic dipole transition moments as functions of the internuclear distance.

R(Å)	$\langle b^1\Sigma_g^+ L X^3\Sigma_{g,M_s=\pm 1}^- \rangle$ (i a.u.)	$\langle b^1\Sigma_g^+ S X^3\Sigma_{g,M_s=\pm 1}^- \rangle$ (i a.u.)	$\langle b^1\Sigma_g^+ M X^3\Sigma_{g,M_s=\pm 1}^- \rangle$ (i μ_B)	$\langle a^1\Delta_g L X^3\Sigma_{g,M_s=\pm 1}^- \rangle$ (i a.u.)	$\langle a^1\Delta_g M X^3\Sigma_{g,M_s=\pm 1}^- \rangle$ (i μ_B)
1.5	0.020765	0.060717	0.142199	0.020114	0.020114
1.7	0.024100	0.068487	0.161075	0.023092	0.023092
1.752	0.025084	0.070752	0.166587	0.023996	0.023996
1.800	0.025882	0.073154	0.172189	0.024779	0.024779
1.82	0.026272	0.074146	0.174564	0.025143	0.025143
1.889	0.027554	0.077828	0.183211	0.026369	0.026369
1.95	0.028579	0.080969	0.190517	0.027407	0.027407
2	0.029324	0.084301	0.197926	0.028197	0.028197
2.02	0.029593	0.085734	0.201062	0.028492	0.028492
2.1	0.030449	0.092158	0.214766	0.029496	0.029496
2.15	0.030757	0.096839	0.224436	0.029902	0.029902
2.2	0.030805	0.102173	0.235151	0.029974	0.029974
2.4	0.012961	0.133883	0.280727	0.020556	0.020556
2.6	−0.004597	0.202326	0.400056	−0.005300	−0.005300
2.8	−0.019259	0.426683	0.834106	−0.024475	−0.024475
3	−0.050699	2.861899	5.673100	−0.072389	−0.072389

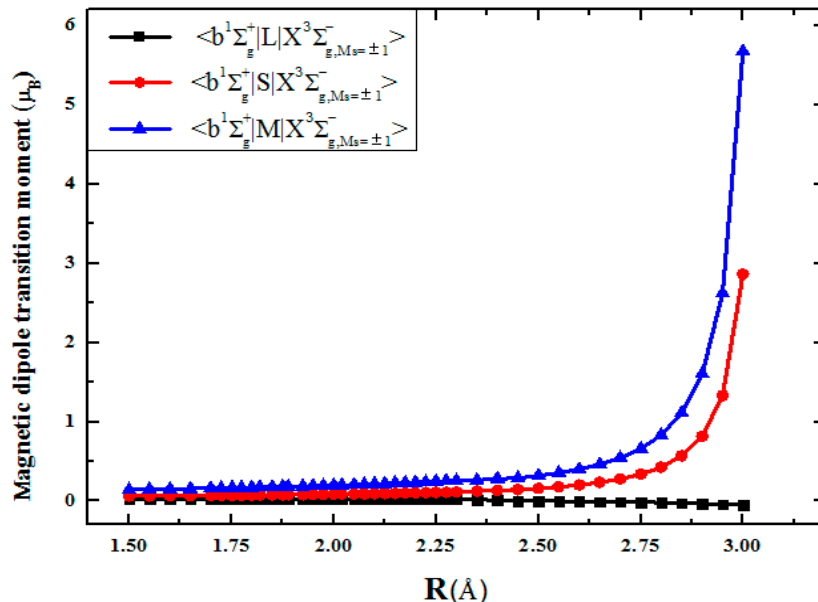


Figure 4. Orbital (L) and spin (S) angular momentum and the total magnetic dipole transition moment contributions to the magnetic $b^1\Sigma_g^+ - X^3\Sigma_{g,M_s=\pm 1}^-$ transition intensity of S_2 .

3.3. Electro-Quadrupole Mechanisms for Transitions between $a^1\Delta_g$ and $X^3\Sigma_g^-$, $b^1\Sigma_g^+$ States in the S_2 Spectrum

According to the selection rules for the electro-quadrupole transition probability ($\Delta\Lambda = 0, \pm 1, \pm 2$, $\Delta S = 0$, g–g, u–u), the transition numbers {3} and {6} are not as effective as magnetic dipole transitions, being extremely weak in the S_2 molecule.

In Figure 5, the quadrupole transition moment of the infrared band $b^1\Sigma_g^+ \rightarrow a^1\Delta_g$ (analogous with the Noxon band of O_2) is calculated as 3.8873 ea₀² at equilibrium in-

ternuclear distance $R_e = 1.889 \text{ \AA}$. Moreover, after considering the SOC effect, the wave functions of the singlet $b^1 \Sigma_g^+$ state and triplet $X^3 \Sigma_g^-$ state are mixed, resulting in the $a^1 \Delta_g - X^3 \Sigma_{g,Ms=0}^-$ transition quadrupole activity. The corresponding electro-quadrupole transition moment to the $\Omega = 0$ component of the ground state $X^3 \Sigma_g^-$ from the $a^1 \Delta_g$ state is equal to $Q_{a-X,0} = -C_{b,X}^* Q_{b-a} = 0.2140 \text{ ea}_0^2$ at the equilibrium distance $R_e = 1.889 \text{ \AA}$.

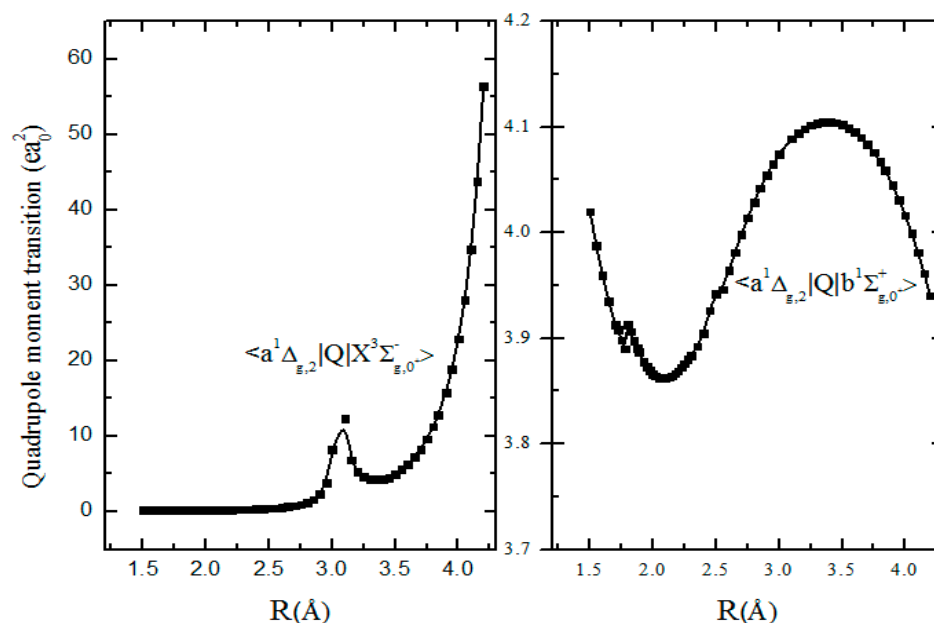


Figure 5. Quadrupole matrix elements of the $a^1 \Delta_g - X^3 \Sigma_{g,Ms=0}^-$ and $a^1 \Delta_g - b^1 \Sigma_g^+$ transitions.

Comparison with the oxygen near IR analogous b–a and a–X,0 bands indicates that the Noxon band in O_2 has comparable intensity with the corresponding S_2 quadrupole transition; their rate constants are 0.0014 and 0.0012 s^{-1} , respectively [41,42]. However, the a–X,0 quadrupole transition which depends on SOC, Equation (9), is much more intense in sulfur dimer than in oxygen. Its rate constant in S_2 is equal to 10^{-5} s^{-1} (Table 5), being impossible to measure in discharge through sulfur vapor. However, an even weaker electric quadrupole contribution to the $a^1 \Delta_g - X^3 \Sigma_g$ transition rate constant in O_2 was identified through its rotational analysis and it was measured this way in order to be equal to $(1.02 \pm 0.10) \times 10^{-6} \text{ s}^{-1}$ [43]. Such a weak oxygen band was detected in the solar absorption spectra because of a long light absorption path through the whole atmosphere [42–44]. The rotational ladder sublevels of the $a^1 \Delta_g$ and $X^3 \Sigma_g$ states can be treated in terms of the Hund’s (b) case coupling [42–44]. The spin sublevels of the ground state in rotating molecules are mixed and more accurate and can be treated in terms of the intermediate Hund’s coupling case [42]. The rotational “e parity” sublevels of the $\Omega = 0$ and $\Omega = 1$ ground $X^3 \Sigma_g$ triplet states are mixed as the spin-rotational terms $F1(J)$ and $F3(J)$; at the same time, the “f parity” rotational sublevel $\Omega = 1$ corresponds to the pure $F2(J)$ rotational term. The rotating molecule wave functions in Equations (2) and (3) depend on rotational quantum number J because of Coriolis coupling $B_e L$ terms [42]. Gordon et al. [44] made a comparison with the low line intensity for the observed P, Q, R branches of the quadrupole a–X transitions of O_2 corresponding to selection rule $\Delta J = \pm 2, \pm 1, 0$, taking into account eigenfunctions of rotational spin sublevels. Good agreement is obtained assuming that the a–X transitions occur only from the SOC-induced mixing between the b and X0 states, as shown in Equation (2), and through intensity borrowing from the Noxon-type band in the oxygen spectrum [42–45]. Thus, similar predictions could be relevant for the quadrupole lines in sulfur dimer a–X absorption (or emission) since their intensity is predicted to be 10 times more efficient with our calculation.

Table 5. Energy (ΔE) of the (0,0) vibrational band, its Einstein coefficient (A), wavelengths (λ), the Franck-Condon factor, and radiative lifetime (τ) of the (0,0) vibrational transition.

Ω - Ω Transition	$\Delta E/\text{cm}^{-1}$	A/s^{-1}	λ/nm	FCF	τ/s
$b^1 \Sigma_g^+ - X^3 \Sigma_{g,Ms=\pm 1}^-$	7641 7961 Expt [24]/7981 Expt [39] 8970 [21] ^a	0.403824 0.423 [21] ^a / 0.3 [21] ^b	1308.94	0.9100	2.4763 2.4 [21] ^a / 3.4 [21] ^b
$a^1 \Delta_g - X^3 \Sigma_{g,Ms=\pm 1}^-$	4197 5551 [21] ^a 4700 Expt [24]	0.001386 0.00286 [21]	2382.95	0.9702	721.2904 350 [21] ^a
$a^1 \Delta_g - b^1 \Sigma_g^+$	3443 3419 [21] ^a / 3617 [21] ^c / 3586 [5,39] ^d	0.001228	2904.68	0.9820	814.1196 960 [21] ^a / 745 [21] ^c / 780 [21] ^d
$a^1 \Delta_g - X^3 \Sigma_{g,Ms=0}^-$	4221	0.000010	2369.65	0.9705	1618.42

^a MRD CI method. ΔE (vertical energy)/ τ (radiative lifetime). ^b This value is obtained by employing the experimental energy difference $\Delta E = 7981 \text{ cm}^{-1}$ and other parameters. Other parameters are from Ref [21] ^c Full CI method. ΔE (vertical energy)/ τ (radiative lifetime) ^d This value is obtained by employing the experimental energy difference $\Delta E = 3586 \text{ cm}^{-1}$ and other parameters. Other parameters are from Ref [21].

The emission probabilities for $b-X_{Ms=\pm 1}$, $a-X_{Ms=\pm 1}$, $b-a$, $a-X_{Ms=0}$ bands of the S_2 spectrum are calculated in Table 5. The Einstein coefficient of the (0, 0) vibrational band for the $b-X_{Ms=\pm 1}$ transition is evaluated as 0.403824 s^{-1} ($\tau = 2.4763 \text{ s}$), which is obtained by employing the calculated energy of the (0, 0) vibrational band ($\Delta E = 7641 \text{ cm}^{-1}$). The experimental value $\Delta E_{0,0} = 7981 \text{ cm}^{-1}$ [39] and theoretical value $\Delta E_{\text{vertical}} = 8970 \text{ cm}^{-1}$ [21] were employed to obtain $A_{0,0}$ by R. Klotz [21], who deduced that $A_{0,0}$ is equal to 0.3 s^{-1} and 0.423 s^{-1} , respectively. Our transition probabilities are closer to the experimental results [21]. In addition, the errors of all these parameters are determined and listed in Table S3. The maximum errors of ΔE_{b-X} and $C_{b,X}$ are 1.86 cm^{-1} and $0.000037i$, respectively. By using the error propagation formula, the error of the Einstein coefficient (ΔA) is calculated to be $\pm 0.0003218 \text{ s}^{-1}$; thus, the typical relative error of A is about 0.08%.

Moreover, the radiative lifetime of the $a^1 \Delta_g - X^3 \Sigma_{g,Ms=\pm 1}^-$ transition is 721.3 s, which is significantly larger than the previous theoretical value (350 s) [21]. The main reason is that the energy difference between our result and the theoretical value [21] is about 1354 cm^{-1} . All the above conclusions imply the fact that the emission probability is sensitive to energy differences; thus, it is important to use precise energy for the spectroscopic predictions.

The probabilities of the electro-quadrupole transition between $a^1 \Delta_g$ and $b^1 \Sigma_g^+$ are determined as $A_{0,0} = 0.001228 \text{ s}^{-1}$ and $\tau_{0,0} = 814 \text{ s}$. The previous radiative lifetime has been calculated by Klotz as 960 s with the MRD CI method or 745 s with the full CI method [21]; and the $\tau_{0,0}$ has been estimated to be 780 s with the experimental energy ($\Delta E = 3586 \text{ cm}^{-1}$) [5,39] in the calculation [21]. In spite of the fact that the Einstein coefficient of the (0, 0) vibrational band of the electric-quadrupole $a^1 \Delta_g - X^3 \Sigma_{g,Ms=0}^-$ transition is very small ($A = 0.000010 \text{ s}^{-1}$), the comparison with the corresponding oxygen analog [42] allows us to predict all quantitative details of its rovibronic structure. It is known that the quenching of the $b^1 \Sigma_g^+$ state in group VI diatomic molecules by foreign gases proceeds mostly by the near-resonant e-to-v energy transfer also involving the spin-allowed quadrupole $b \rightarrow a$ transition [23,43]. The late mechanism is very important because of intense electric dipole-quadrupole intermolecular interactions [43]. Moreover, the $a^1 \Delta_g$ state quenching by intermolecular electronic-to-vibrational (e-to-v) energy transfer depends on the SOC-induced quadrupole $a \rightarrow X,0$ transition [43,46,47]; thus, the exact knowledge of quadrupole moments is important.

The 0–0, 0–1, and 1–1 bands of the $b-X_{Ms=\pm 1}$ emission system were measured by Fink [22,41], who monitored the 0–0 band at $1.25 \mu\text{m}$ through a Bomem interferometer in the near-infrared spectral region. the molecular constants for the 0–0, 0–1, and 1–1 bands of the $b-X_{Ms=\pm 1}$ transition are obtained from by Fink [22]. The intensity of the magnetic transition for the 0–0 band of the $a-X_{Ms=\pm 1}$ system is very low, and the Einstein coefficient is equal to about 0.001386 s^{-1} ; in fact, it is hard to measure. However, Setzer [23] observed the weak band (0–0 band of the $a-X_{Ms=\pm 1}$ transition) of this chemically unstable molecule

S_2 near 4400 cm^{-1} in the early low-resolution emission study. In Figure 6, we give the transition intensity represented by the experimentally observed vibrational $b-X_{Ms=\pm 1}$ and $a-X_{Ms=\pm 1}$ bands. Each vertical line represents a vibration energy level band; in order to see each vibrational level more clearly, we use different colors to represent the corresponding bands of different vibrational levels; the ordinate and abscissa represent its transition intensity and band energy position, respectively.

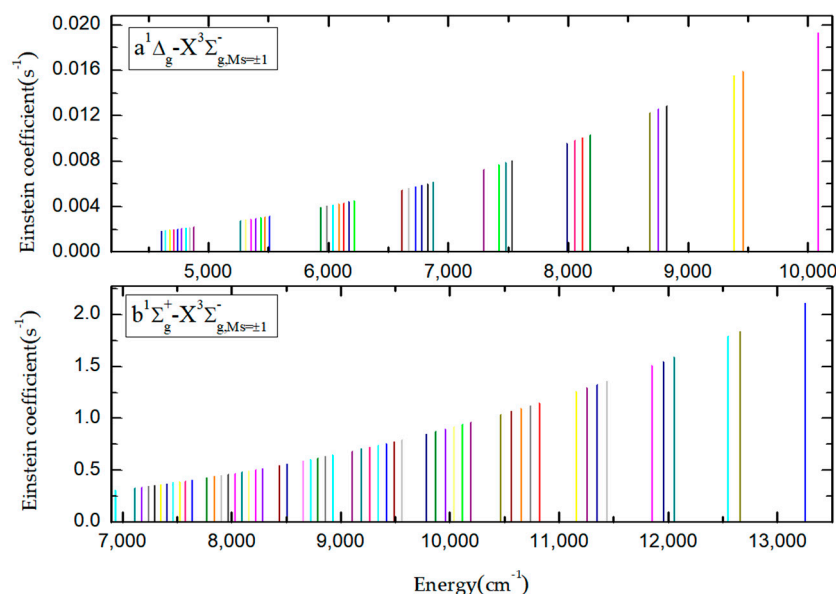


Figure 6. Theoretically inferred experimental vibrational bands.

In order to provide more observable bands for the experiment, we take the intensity of $b-X_{Ms=\pm 1}$ (0, 0) and $a-X_{Ms=\pm 1}$ (0, 0) bands as the zero point of the abscissa, respectively. This will prove that the above bands can be detected by modern optical facilities and spectral resolution presented in Figure 6; the relevant experimentally observed vibrational energy band information—including the vibrational levels, Einstein coefficients, and oscillator strengths—are listed in Tables S4 and S5 of the Supplementary Material. Comparison with previous theoretical studies [20,21] indicates that the increase of the basis set and active space of the MRCI method is important for a detailed understanding of spectral peculiarities in the forbidden bands of the sulfur dimer.

The studied forbidden bands in the S_2 spectrum finalize a series of magnetic and quadrupole transition calculations in diatomic molecules [42,47,48]. Despite relatively low intensity and experimental difficulties in their detection, the theoretical studies of the magnetic and quadrupole transitions are important for astrophysical studies and for fundamental knowledge of molecular structure in physical chemistry [48].

4. Conclusions

Transitions from the $b^1\Sigma_g^+$ and $a^1\Delta_g$ states to the ground state $X^3\Sigma_g^-$ are forbidden in the framework of electric dipole selection rules for the S_2 molecule. The present paper has estimated the intensity of the parity-forbidden singlet-triplet (S–T) transitions of the S_2 molecule for the inter-combinations between groups of states $a^1\Delta_g$, $b^1\Sigma_g^+$ and $X^3\Sigma_g^-$ in the near-IR region by employing high-level ab initio MRCI calculations with the SOC and CV correlation. The radiative lifetime of the $b^1\Sigma_g^+ - X^3\Sigma_{g,Ms=\pm 1}^-$ transition is largely determined by spin angular-momentum term contributions to the magnetic moment, due to the zero-field splitting of the $X^3\Sigma_g^-$ state for S_2 . The intensity of the $a^1\Delta_g - X^3\Sigma_{g,Ms=\pm 1}^-$ transition is dominated by the orbital part in the magnetic dipole transition, and it arises from the $a^1\Delta_g - ^3\Pi_g$ and $X^3\Sigma_g^- - ^1\Pi_g$ transitions. Comparing with the radiative lifetimes of the electro-quadrupole transition for the $a^1\Delta_g - b^1\Sigma_g^+$ band, our result was found to be within a reasonable error of existing calculations. Though the electro-quadrupole

transition is almost negligible for the $a^1\Delta_g - X^3\Sigma_{g,M_s=0}^-$ (0,0) band (either in emission or in absorption), comparison with the analogous oxygen near-IR spectrum [44] indicates the detailed prediction for more intense quadrupole branches in rotational structure ratios for the S_2 molecule.

The current results show that the experimentally detected 0–0, 0–1, and 1–1 bands of the $b^1\Sigma_g^+ - X^3\Sigma_{g,M_s=\pm 1}^-$ emission system [22,41] are well reproduced by ab initio theory. There is no doubt that we also fully calculate and interpret the weak 0–0 vibrational band of the $a^1\Delta_g - X^3\Sigma_{g,M_s=\pm 1}^-$ transition for chemically unstable S_2 molecules experimentally studied by Setzer and Fink [23]. We also successfully provide some other bands for the magnetic IR spectrum of the S_2 dimer. A preliminary attempt to calculate the low transition probabilities of the $b-X_{M_s=\pm 1}$, $a-X_{M_s=\pm 1}$, $b-a$, $a-X_{M_s=0}$ bands with the perturbation theory formulas was satisfactory. Our study of the S_2 molecular spectrum in the near-IR region provides more useful information for the exploration of matter in the field of astrophysics. This study provides the systematic calculations of forbidden magnetic and quadrupole transitions in O_2 , N_2 , Ge_2 , and Sn_2 homonuclear diatomic molecules and illustrates the increasing role of spin-orbit coupling effects in such fields of physical chemistry.

Supplementary Materials: The following supporting information can be downloaded at: <https://www.mdpi.com/article/10.3390/physchem3010009/s1>, Table S1: The vertical excitation energies with the $X^3\Sigma_g^-$ state for other states (cm^{-1}) in $R_{s-s} = 1.899\text{\AA}$; Table S2: Calculated spin-orbit matrix elements in $S_2(R_{s-s} = 1.899\text{\AA})$; Table S3: The error analysis for the Einstein coefficient A of the $b-X_{M_s=0}$ transition; Table S4: The theoretically inferred energy, Einstein coefficient and oscillator strength of the experimentally observable $b-X_{M_s=\pm 1}$ band; Table S5: The theoretically inferred energy, Einstein coefficient and oscillator strength of the experimentally observable $a-X_{M_s=\pm 1}$ band.

Author Contributions: Conceptualization: L.X., B.Y. and B.F.M.; methodology: L.X., B.Y. and B.F.M.; formal analysis: L.X., B.Y. and B.F.M.; original draft preparation: L.X. All authors have read and agreed to the published version of the manuscript.

Funding: This work was supported by the National Natural Science Foundation of China (Grant No. 12274178, No. 11874177, and No. 11574114); the Ministry of Education and Science of Ukraine (Grant No. 0121U107533); the Wenner-Gren Foundation (Grant No. GFU2022-0036); the High Performance Computing Center (HPCC) of Jilin University and the high performance computing cluster Tiger@ IAMP.

Data Availability Statement: The data presented in this study are available in article and supplementary material.

Conflicts of Interest: The authors declare no conflict of interest.

References

1. Fowler, A.; Vaidya, W.M. The Spectrum of the Flame of Carbon Disulphide. *Proc. R. Soc. London. Ser. A Contain. Pap. A Math. Phys. Character* **1931**, *132*, 310–330.
2. Tanaka, Y.; Ogawa, M. Emission spectrum of S_2 in the vacuum ultraviolet region. *J. Chem. Phys.* **1962**, *36*, 726–730. [CrossRef]
3. Maeder, R.; Miescher, E. Absorption band spectrum of S_2 in the Schumann region. *Nature* **1948**, *161*, 393. [CrossRef] [PubMed]
4. Bondybey, V.E.; English, J.H. $B^3\Sigma_u^-$ predissociation and relaxation processes in matrix isolated S_2 . *J. Chem. Phys.* **1979**, *72*, 3113–3122. [CrossRef]
5. Yuan, D.F.; Trabelsi, T.; Zhang, Y.R.; Francisco, J.S.; Wang, L.S. Probing the Electronic Structure and Bond Dissociation of SO_3 and SO_3^- Using High-Resolution Cryogenic Photoelectron Imaging. *J. Am. Chem. Soc.* **2022**, *144*, 13740–13747. [CrossRef] [PubMed]
6. Reddy, R.R.; Rama, G.K.; Nazeer, A.Y.; Baba, B.D.; Narasimhulu, K.; Siva Sankar Reddy, L. Spectroscopic studies of molecules observed in comets. *Indian J. Pure Ap. Phy.* **2005**, *43*, 237–245.
7. De Almeida, A.A.; Singh, P.D. Photodissociation lifetime of $^{32}S_2$ molecule in comets. *Earth Moon Planets* **1986**, *36*, 117–125. [CrossRef]
8. Spencer, J.R.; Jessup, K.L.; McGrath, M.A.; Ballester, G.E.; Yelle, R. Discovery of gaseous S_2 in Io's Pele plume. *Science* **2000**, *288*, 1208–1210. [CrossRef]
9. Xue, J.L.; Yuan, X.; Li, R.; Liu, X.S.; Yan, B. Theoretical study on predissociation of $B^3\Sigma_u^-$ of sulfur dimer. *Spectrochim. Acta Part A Mol. Biomol. Spectrosc.* **2020**, *241*, 118679. [CrossRef]

10. Kiljunen, T.; Eloranta, J.; Kunttu, H.; Khriachtchev, L.; Pettersson, M.; Räsänen, M. Electronic structure and short-range recombination dynamics of S₂ in solid argon. *J. Chem. Phys.* **2000**, *112*, 7475–7483. [\[CrossRef\]](#)
11. Frederix, P.W.J.M.; Yang, C.H.; Groenenboom, G.C.; Parker, D.H.; Alnama, K.; Western, C.M. Photodissociation imaging of diatomic sulfur (S₂). *J. Phys. Chem. A* **2009**, *113*, 14995–15005. [\[CrossRef\]](#) [\[PubMed\]](#)
12. Yamashita, J.; Fujihara, K.; Takahashi, O.; Kohguchi, H.; Yamasaki, K. Kinetics and dynamics on the formation of S₂(X³Σ[−]_g−a¹Δ_g) in the S(¹D) + OCS reaction. *J. Phys. Chem. A* **2014**, *118*, 9330–9337. [\[CrossRef\]](#) [\[PubMed\]](#)
13. Green, M.E.; Western, C.M. Upper vibrational states of the B³Π_u state of ³²S₂. *J. Chem. Soc. Faraday Trans.* **1997**, *93*, 365–372. [\[CrossRef\]](#)
14. Minaev, B.F.; Minaeva, V.A. MCSCF response calculations of the excited states properties of the O₂ molecule and a part of its spectrum. *Phys. Chem. Chem. Phys.* **2001**, *3*, 720–729. [\[CrossRef\]](#)
15. Wieland, K. Thermo-optical dissociation of sulphur dioxide. *Trans. Faraday Soc.* **1934**, *30*, 260–265. [\[CrossRef\]](#)
16. Donovan, R.J.; Husain, D.; Jackson, P.T. Transient species in the photolysis of sulphur monochloride, including S₂ (a¹Δ_g). *Trans. Faraday Soc.* **1968**, *64*, 1798–1805. [\[CrossRef\]](#)
17. Chiang, S.Y.; Lee, Y.P. Red and near-infrared laser-induced emission of S₂ in an Ar matrix. *J. Chem. Phys.* **1988**, *89*, 13–19. [\[CrossRef\]](#)
18. Minaev, B.F. Intensity of singlet-triplet transitions in the oxygen molecule and the selective effect of an external heavy atom. *Opt. Spectrosc.* **1978**, *45*, 1202–1207.
19. Minaev, B.F. Electronic mechanisms of activation of molecular oxygen. *Russ. Chem. Rev.* **2007**, *76*, 1059. [\[CrossRef\]](#)
20. HESS, B.A.; Buenrer, R.J. Ab initio calculation of the Zero-Field splittings of the X³Σ[−]_g, B³Π_{g,1} states of the S₂ molecule. *Chem. Phys.* **1982**, *71*, 79–85. [\[CrossRef\]](#)
21. Klotz, R.; Marian, C.M.; Peyerimhoff, S.D. Calculation of spin-forbidden radiative transitions using correlated wavefunctions lifetimes of b¹Σ⁺, a¹Δ states in O₂, S₂ and SO. *Chem. Phys.* **1984**, *89*, 223–236. [\[CrossRef\]](#)
22. Fink, E.H.; Kruse, H.; Ramsay, D.A. The high-resolution emission spectrum of S₂ in the near infrared, The b¹Σ⁺_g−X³Σ[−]_g system. *J. Mol. Spectrosc.* **1986**, *119*, 377–387. [\[CrossRef\]](#)
23. Setzer, K.D.; Kalb, M.; Fink, E.H. The a¹Δ_g−X³Σ[−]_g magnetic dipole transition of S₂. *J. Mol. Spectrosc.* **2003**, *221*, 127–130. [\[CrossRef\]](#)
24. Barnes, I.; Becker, K.H.; Fink, E.H. Near-infrared emissions from the ¹Δ_g and ¹Σ⁺_g states of S₂. *Chem. Phys. Lett.* **1979**, *67*, 314–317.
25. Fink, E.H.; Kruse, H.; Setzer, K.D. High resolution fourier-transform spectra of the a¹Δ_g−X³Σ[−]_g, b¹Σ⁺_g−X³Σ[−]_g and b¹Σ⁺_g−a¹Δ_g systems of O₂, SO, S₂ and isoelectronic molecules in the nir region. *Acta Phys. Hung.* **1990**, *67*, 67–72. [\[CrossRef\]](#)
26. Werner, H.J.; Knowles, P.J.; Knizia, G.; Manby, F.R.; Schütz, M. Molpro: A general-purpose quantum chemistry program package. *W. I. Res. Comput. Mol. Sci.* **2012**, *2*, 242–253. [\[CrossRef\]](#)
27. A'Hearn, M.F.; Feldman, P.D.; Schleicher, D.G. The discovery of S₂ in comet IRAS-Araki-Alcock 1983d. *Astrophys. J.* **1983**, *274*, L99–L103. [\[CrossRef\]](#)
28. Epler, J.E.; Verdeyen, J.T. Broad-Band Gain in Optically Pumped S₂. *IEEE J. Quantum Elect.* **1983**, *19*, 1686–1691. [\[CrossRef\]](#)
29. Glassgold, A.E. Circumstellar photochemistry. *Annu. Rev. Astron. Astr.* **1996**, *34*, 241–277. [\[CrossRef\]](#)
30. Grim, R.J.A.; Greenberg, J.M. Photoprocessing of H₂S in interstellar grain mantles as an explanation for S₂ in comets. *Astron. Astrophys.* **1987**, *181*, 155–168.
31. Kim, S.J.; A'Hearn, M.F.; Larson, S.M. Multi-cycle fluorescence, Application to S₂ in comet IRAS-Araki-Alcock 1983VII. *Icarus* **1990**, *87*, 440–451. [\[CrossRef\]](#)
32. Lewis, J.S.; Kreimendahl, F.A. Oxidation state of the atmosphere and crust of Venus from pioneer Venus results. *Icarus* **1980**, *42*, 330–337. [\[CrossRef\]](#)
33. Liszt, H.S. Upper limits on the abundance of the sulfur dimer in molecular clouds. *Astrophys. J.* **1978**, *219*, 454–457. [\[CrossRef\]](#)
34. Mitchell, G.F. Effects of shocks on the sulfur chemistry of a dense interstellar cloud. *Astrophys. J.* **1984**, *287*, 665–670. [\[CrossRef\]](#)
35. Noll, K.S.; McGrath, M.A.; Trafton, L.M.; Atreya, S.K.; Caldwell, J.J.; Weaver, H.A. HST spectroscopic observations of Jupiter after the collision of comet Shoemaker—Levy 9. *Science* **1995**, *267*, 1307–1313. [\[CrossRef\]](#) [\[PubMed\]](#)
36. Shnitko, I.; Fulara, J.; Garkusha, I.; Nagy, A.; Maier, J.P. Electronic transitions of S₂[−] and S₃[−] in neon matrixes. *Chem. Phys.* **2008**, *346*, 8–12.
37. Huber, K.P.; Herzberg, G. *Constants of Diatomic Molecules*; Van Nostrand Reinhold Co.: New York, NY, USA, 1979.
38. Swope, W.C.; Lee, Y.P.; Schaefer, H.F., III. Diatomic sulfur: Low lying bound molecular electronic states of S₂. *J. Chem. Phys.* **1979**, *70*, 947–953. [\[CrossRef\]](#)
39. Bielefeld, M.; Elfers, G.; Fink, E.H.; Kruse, H.; Wildt, J.; Winter, R. O₂(a¹Δ_g)-sensitized chemiluminescence of a¹Δ → X³Σ[−] and b¹Σ⁺ → X³Σ[−] transitions of group VI—Group VI and group V—group VII diatomic molecules. *J. Photoch.* **1984**, *25*, 419–438. [\[CrossRef\]](#)
40. Veillard, A. Gaussian basis set for molecular wavefunctions containing second-row atoms. *Theo. Chim. Acta* **1968**, *12*, 405–411. [\[CrossRef\]](#)
41. Fink, E.H.; Setzer, K.D.; Kottsieper, U.; Ramsay, D.A.; Vervloet, M. The a¹Δ (a₂)—X³Σ[−] (X₂1) electronic band system of selenium monoxide. *J. Mol. Spectrosc.* **1988**, *131*, 127–132. [\[CrossRef\]](#)
42. Minaev, B.F.; Murugan, N.A.; Ågren, H. Dioxygen spectra and bio-activation. *Int. J. Quant. Chem.* **2013**, *113*, 1847–1867. [\[CrossRef\]](#)

43. Sveshnikova, E.B.; Minaev, B.F. Mechanism of the nonradiative $^1\Delta_g - ^3\Sigma_g^-$ transition in molecular oxygen in solution. *Opt. Spectrosc.* **1983**, *54*, 320–322.
44. Gordon, I.E.; Kass, S.; Campargue, A.; Toon, G.C. First identification of the $a^1\Delta_g - X^3\Sigma_g^-$ electric quadrupole transitions of oxygen in solar and laboratory spectra. *J. Quant Spectrosc. Radiat. Transf.* **2010**, *111*, 1174. [[CrossRef](#)]
45. Minaev, B.F. Effect of spin-orbit coupling on the intensity of magnetic dipole transitions in molecular oxygen. *Sov. Phys. J.* **1978**, *21*, 1205–1209, Erratum in *Izv. Vyssh. Uchebn. Zaved. Fiz.* **1978**, *9*, 115. [[CrossRef](#)]
46. Minaev, B.F. Spin-orbit coupling mechanism of singlet oxygen $a^1\Delta_g$ quenching by solvent vibrations. *Chem. Phys.* **2017**, *483*, 84–95. [[CrossRef](#)]
47. Xiao, L.D.; Xue, J.L.; Liu, Y.; Yan, B.; Minaev, B.F. Calculation of the singlet-triplet magnetic and electro-quadrupole transitions intensity for Ge_2 molecule. *Mol. Phys.* **2020**, *120*, e20745622020. [[CrossRef](#)]
48. Minaev, B.F.; Panchenko, O.O.; Minaeva, V.A.; Agren, H. Triplet state harvesting and search for forbidden transition intensity in the nitrogen molecule. *Front. Chem.* **2022**, *10*, 1005684. [[CrossRef](#)] [[PubMed](#)]

Disclaimer/Publisher's Note: The statements, opinions and data contained in all publications are solely those of the individual author(s) and contributor(s) and not of MDPI and/or the editor(s). MDPI and/or the editor(s) disclaim responsibility for any injury to people or property resulting from any ideas, methods, instructions or products referred to in the content.